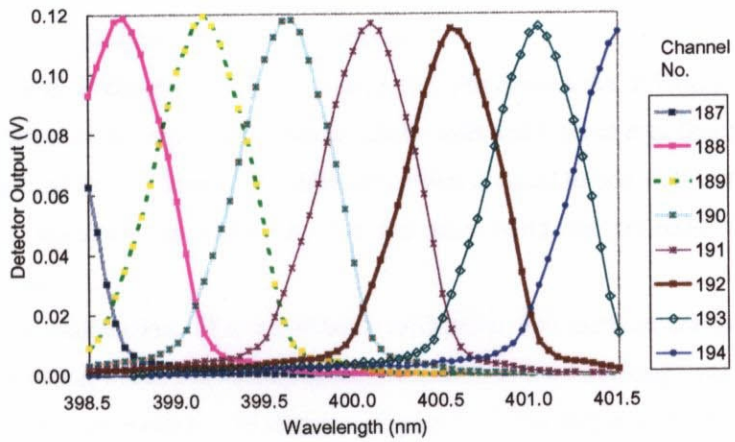

Figure 5-10. The laboratory-model measured slit function without a depolarizer using the 1 m monochromator.

Table 5-7. Four diffuser plate and their operation plan.

	Type	Frequency
1	Sand blasted Al-a	Every sunrise or sunset
2	Sand blasted Al-b	Once a week
3	Sand blasted Al-c	Once a year
4	Spectralon	Once a week at the same time as sand blasted Al-b

Onboard radiometric calibration and diffuse plates operation. The absolute radiometric response and the center wavelength will be calibrated onboard every week. For the radiometric calibration onboard, diffuser plates illuminated by direct solar flux will be used. The 3 sand-blasted Al plates with different exposure time and one spectralon diffuser plate will be integrated into the instrument as summarized in Table 5-7. A spectralon diffuser has an excellent Lambertian surface but can be degraded by UV radiation. On the other hand, an Al plate is electron and UV radiation hardened but has a poorly diffusive surface. As the satellite orbit is non-sun synchronous, the geometry of the input solar radiation and the output reflection to the scan mirror will change with the orbit and so bi-directional reflection distribution function (BRDF) calibration is needed. In addition, the surface of the diffuser plate may be degraded by the contamination radiated by short-wave solar UV on orbit. The 3 Al diffuser plates must be operated carefully because the degradation is assumed to be proportional to the total exposure time. One Al plate is always exposed, while the second Al plate and the spectralon will be used once a week. These two plates are used at the same time for the same exposure time. This operation enables the spectrometer degradation to be discriminated from the diffuser plate degradation. The last Al plate will be used once a year, and is expected not to be degraded during the nominal three years' mission life due to its limited exposure time.

Lunar Calibration. Lunar surface can be assumed to be lambertian and very stable. By rotating the

space craft and pointing the nadir view to the moon, the scatted light on the moon surface can be introduced onto the fore optics. IFOV will cover the whole lunar disk and the input level of the lunar calibration flux is almost same as the scatted light from the earth atmosphere.

Radiation hardness of the diffusers. The solar flux illuminates the diffusers directly. Two radiation sources must be considered as the degradation source: ultra-violet and high-energy fluxes. The BRDF of the Al diffusers were not degraded by 400 hours' UV radiation, which is equal to one year of radiation on the diffuser, and 3×10^{12} e/cm^2 total dose electron radiation. On the other hand, the reflectivity of the spectralon was degraded by UV radiation.

Onboard spectral calibration. For wavelength calibration, two methods are considered. One is to use the Hg lamp emission spectra, which has several emission spectra in the wavelength region. The other is to use the solar Fraunhofer absorption spectra. As shown in Figure 5-11, the output of the Hg lamp is sensitive to the wavelength shift onboard. On the other hand, the Fraunhofer spectra have a random-like structure and finer structure than the spectral sampling interval. As indicated in Figure 5-12, the output is less sensitive, so the Fraunhofer spectra are used as the redundant calibration method. As the temperature of the spectrometer is controlled to keep the temperature change less than 1 degree C, the wavelength shift due to the temperature change during the Hg lamp calibrations will be less than 0.01 nm. Once a wavelength shift over 0.01 nm is detected, the look-up table for data retrieval has to be replaced. Thus, the instrument will provide good wavelength-calibrated data throughout the entire mission.

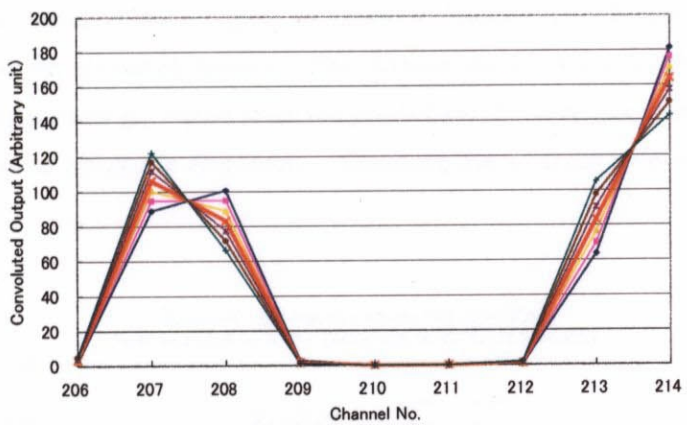

Figure 5-11. Hg lamp sensitivity on the wavelength shift (nominal, +/-1, 2, 3 cm^{-1} (+/-0.016, 0.032, 0.048 nm)).

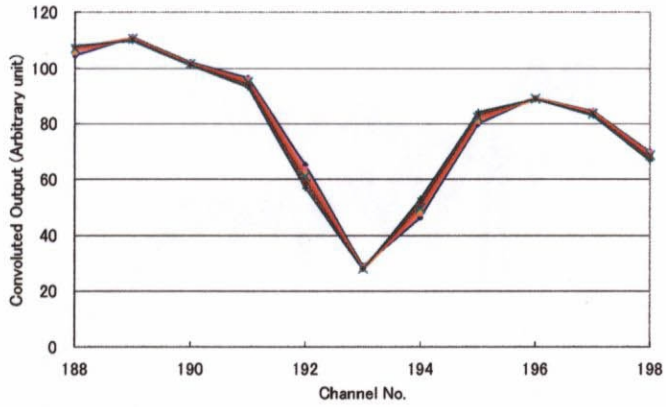

Figure 5-12. Solar Fraunhofer line sensitivity on the wavelength shift (nominal, +/-1, 2, 3 cm^{-1}).

5.6. Test Results

(1) Laboratory model

The laboratory model consists of the first-generation custom-made test detector and the optics using commercial items. The first-generation detector has the uniformly sized pixels (0.26 by 0.26 mm) and pre-fixed gain levels of 0.1 pF, 0.5 pF, and 1 pF for short-, middle-, and long-wavelength pixels. Sky light spectra were acquired on the ground with the same level of the spectral radiance in the long-wave region as in orbit and weaker one in the short-wave region, as shown in Figure 5-13. Figure 5-14 depicts the detector output and the SNR of the measured spectra. The detector does not collect most of the input spectra, particularly in the longer-wavelength region since the pixels have the same size over the whole spectral range and the spectrometer has an astigmatic aberration. Therefore, the achieved SNR was low and the pixel size had to be modified.

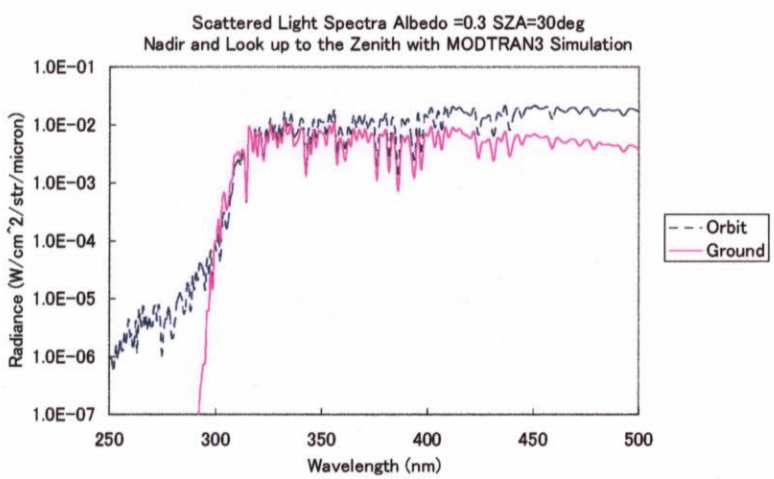

Figure 5-13. Simulated scattered light spectra from orbit (dotted line) and on the ground (solid line) by MODTRAN.

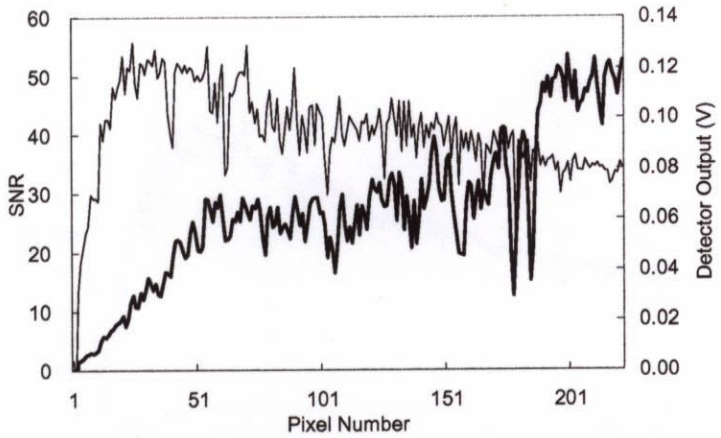

Figure 5-14. Detector output of the skylight measurement (bold line) and SNR (solid line) acquired with the laboratory model on 10 January, 1998 in Yokohama.

(2) Design upgrade and engineering model test results

The data acquired using the engineering model optics and array detector package is presented in Figure 5-15. This detector has a different pixel height that is greater in the longer-wavelength to collect most of the input photons, and the gain level can be set to 0.1 pF or 1 pF. The result yields a fine solar Fraunhofer line structure looking at the zenith sky with a 0.5 nm step. Figure 5-16 displays the achieved SNR. The SNR is highest between 320 and 350 nm, where the total O_3 is retrieved. The SNR in the shorter-wavelength region is significantly increased by collecting as much of the photon flux as possible, compared with the laboratory model results. The SNR level decreases in the longer-wavelength region due to the detector noise of the lager area of the pixels. The SNR is expected to be improved in the longer-wavelength region by insertion of an aberration collection cylindrical lens. Figure 5-17 presents the raw skylight spectra using the engineering model optics and detector measured on the ground compared with the MODTRAN4 simulation. The results demonstrate that the instrument has good spectral resolution as designed.

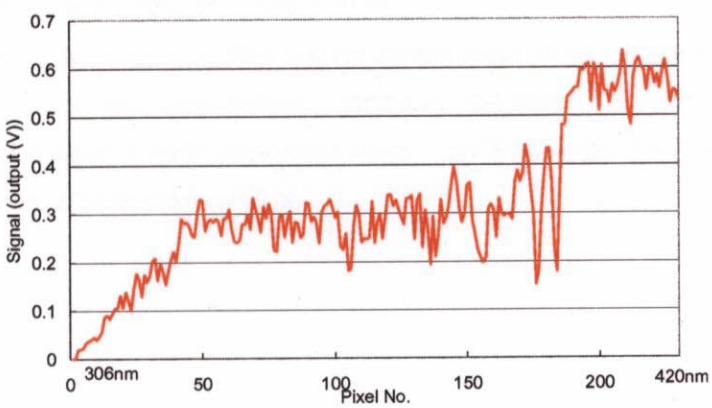

Figure 5-15. The raw skylight spectra using the engineering model optics and detector measured on the ground.

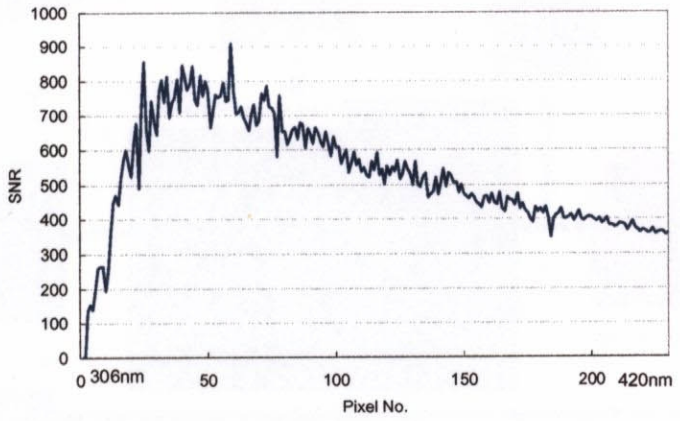

Figure 5-16. The same as Figure 5-15 except for the acquired SNR.

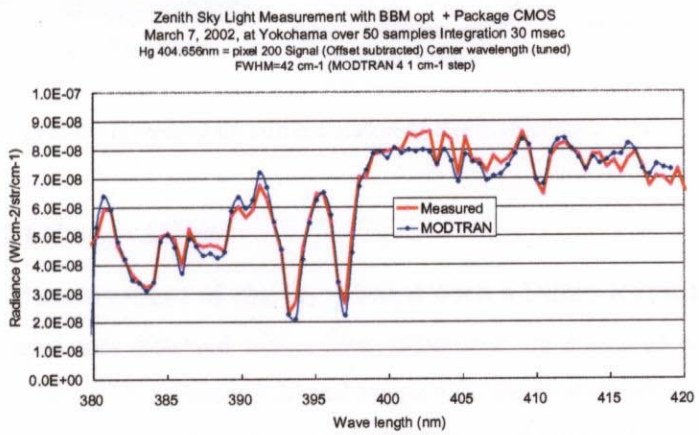

Figure 5-17. Skylight raw spectra using the engineering model optics and detector measured on the ground compared with MODTRAN4 simulation.

(3) Integration of the space qualified components

Figure 5-18 illustrates the integration flow and the current status of the components. Most components of the engineering model have been manufactured, integrated, and tested. A spectrometer with a detector tested in a vacuum chamber under a wide temperature range. No wavelength shift was detected, and this test results verify its superior on-orbit thermal stability.

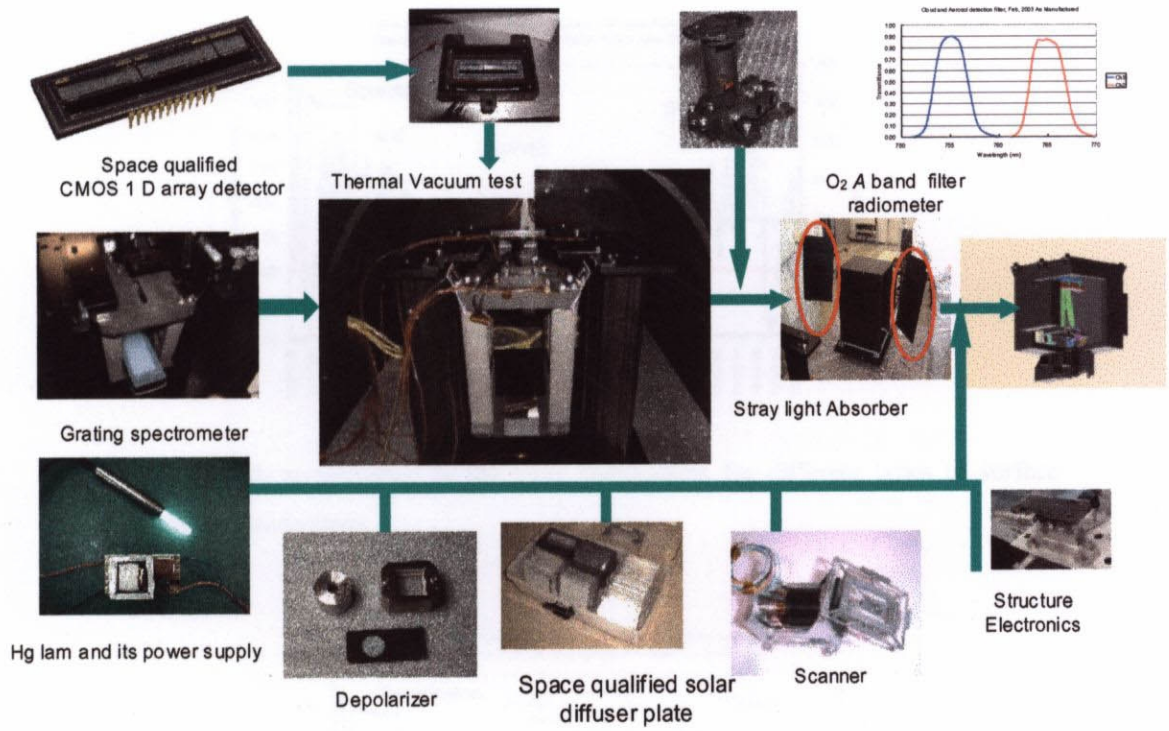

Figure 5-18. The integration flow and its current status of the instrument.

5.7. Ground-based Observation

5.7.1. Ground-based Measurement of the O_2 *A* band with a Filter Radiometer

The O_2 *A* band measured data observed with a filter radiometer are displayed in Figure 5-19 together with the 4 cm^{-1} spectral resolution FTS. Figure 5-20 and Figure 5-21 depict the SNR performance of the filter radiometer for different types of surface-scattered light measurements and retrieved optical thicknesses from in and out of the O_2 *A* band data. The results verify the very high SNR. However, the optical thickness still requires correction. The difference between the targets is thought to be due to the misalignment of the field of view between the two bands.

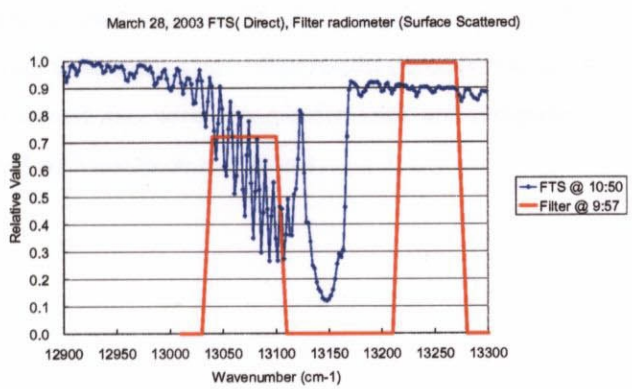

Figure 5-19. O_2 *A* band measured data with two filter radiometers and a FTS.

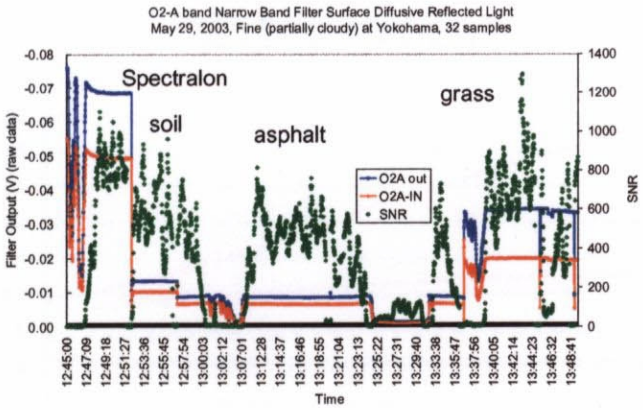

Figure 5-20. SNR performance of the filter radiometers for different types of surface scattered light measurements.

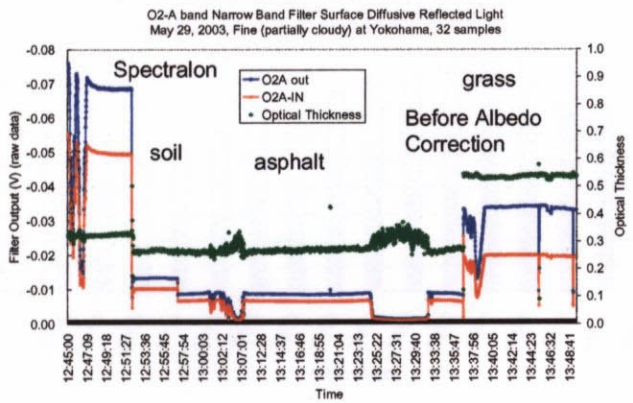

Figure 5-21. Retrieved optical thickness from 2 bands of filter radiometers for different types of surface scattered light measurements.

5.7.2. Ground-based Measurement of O_3 Absorption Spectra

Figure 5-22 displays the measured spectra ratio of the sunset spectra to that at the noon acquired with the engineering model on the ground on November 27, 2002, together with the simulated effective airmass factor and scattered light contribution from each layer. The results demonstrate that the spectra of the O_3 absorption cross section are clearly observed and solar Fraunhofer lines are completely removed. This indicates no wavelength shift was detected between noon and sunset.

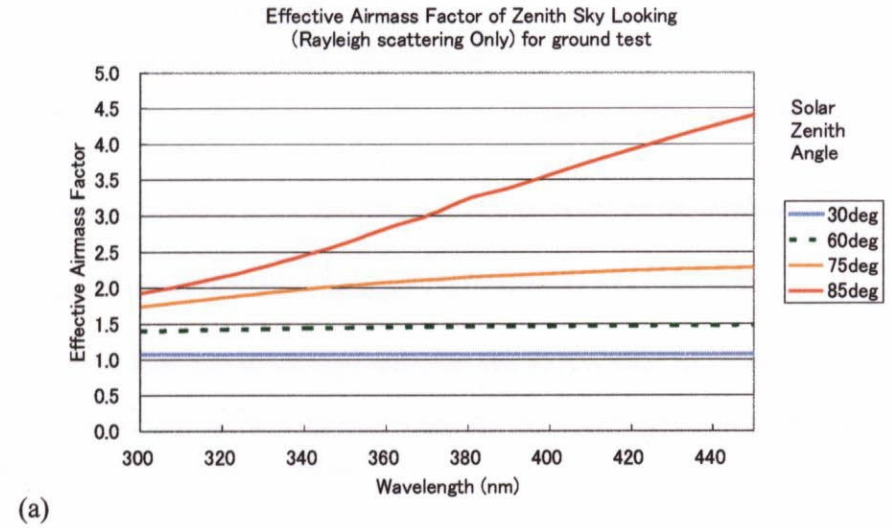

(a)

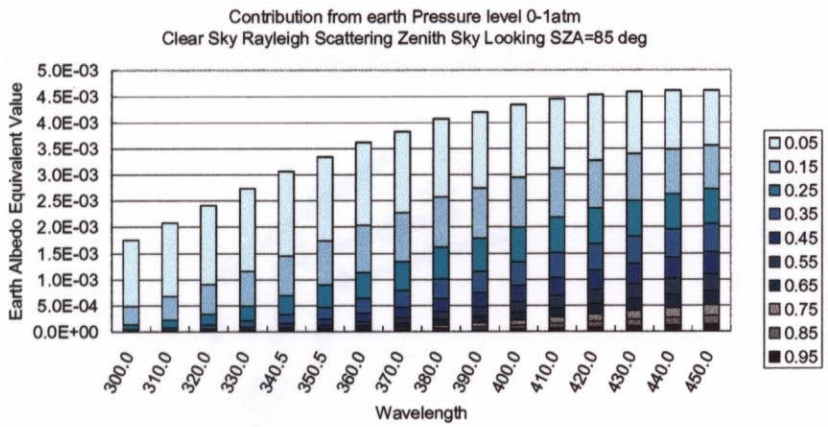

(b)

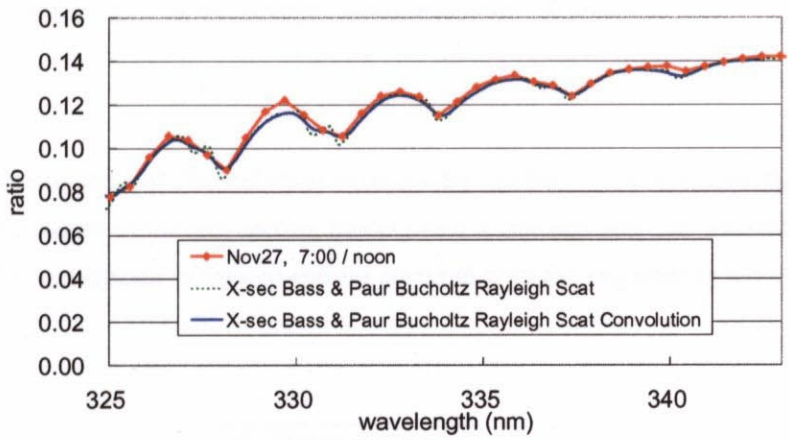

(c)

Figure 5-22. Measured spectra ratio of the sunset spectra to the one of the noon acquired with the engineering model on the ground on November 27, 2002: (a) the spectral characteristics of the effective air-mass factor for solar zenith angles of 30, 60, 75, and 80 degrees, (b) contribution from each layer, and (c) comparison between measurements and model simulation.

5.7.3. Ground-based Measurement of NO_2

(1) Measurement geometry and model calculation

The skylight spectra were measured under the same integration time as in orbit, as schematically illustrated in Figure 5-23.

The expected measured skylight under the clear sky conditions can be modeled as

$$I_\lambda = \frac{1}{4\pi} F_\lambda \beta_{Rayleigh\lambda} P(\cos\theta_0) \int_0^1 exp\left[-\left(\beta_{Rayleigh\lambda}(p/\cos(SZA)+(1-p))\right)\right]dp, \quad (5\text{-}1)$$

where $\beta_{Rayleigh}$ is the Rayleigh scattering coefficient and SZA is solar zenith angle.

Mie scattering from the sky will be dominant when the thin clouds or aerosols exist, and the measured scattered light from the zenith sky is described as,

$$I_\lambda = \frac{1}{4\pi} F_\lambda \beta_{Mie\lambda} P_{Mie}(\cos\theta_0) exp\left[-\left(\beta_{Rayleigh\lambda}(p_{cloud}/\cos(SZA)+(1-p_{cloud}))\right)\right], \quad (5\text{-}2)$$

where β_{Mie} is the Mie scattering coefficient and P_{cloud} is the cloud layer pressure.

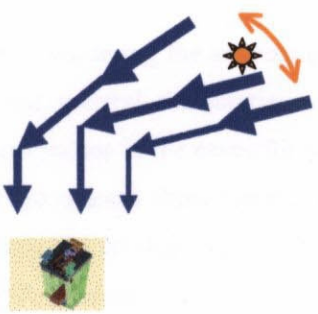

Figure 5-23. Schematic figure of the skylight measurement on the ground.

(2) Measured data

The wavelength of each spectral channel must be characterized before the scattered light is measured. Figure 5-24 presents the output of the engineering model using a mercury lamp for wavelength calibration. Figure 5-25 presents the wavelength-calibrated spectra acquired with the engineering model on the ground on November 27, 2002.

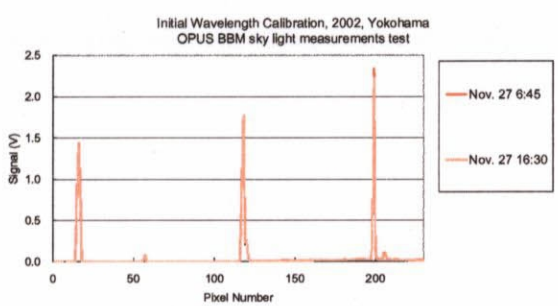

Figure 5-24. Wavelength calibration of the engineering model using a mercury lamp.

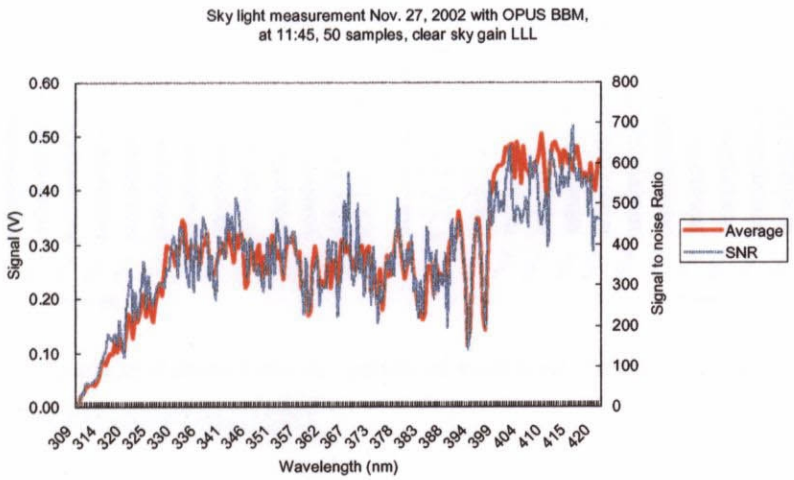

Figure 5-25. Wavelength-calibrated spectra acquired with the engineering model on the ground on November 27, 2002.

(3) Correction

The effective air mass must be calculated considering the scattering from each layer to estimate the vertical column densities. Figure 5-26 depicts the spectral characteristic models of Mie and Rayleigh scattering coefficients and the earth albedo equivalent values in the cases for solar zenith angles of 60 deg (left) and 80 deg (right). Figure 5-27 presents shows the spectral characteristic models of each layer's contribution in the cases of solar zenith angles of 60 deg (left) and 80 deg (right). Figure 5-28 displays the effective air-mass factor at 420 nm for the November 27, 2002, observation.

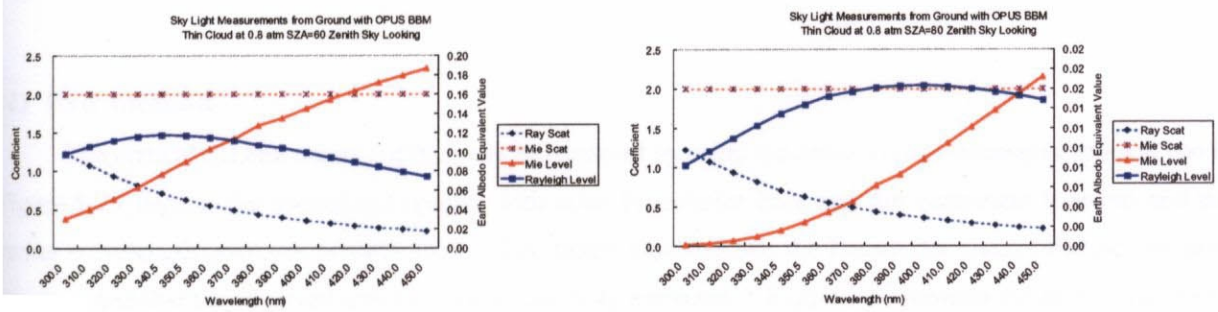

Figure 5-26. The spectral characteristics models of Mie and Rayleigh scattering coefficients for the solar zenith angles of 60 deg (left) and 80 deg (right).

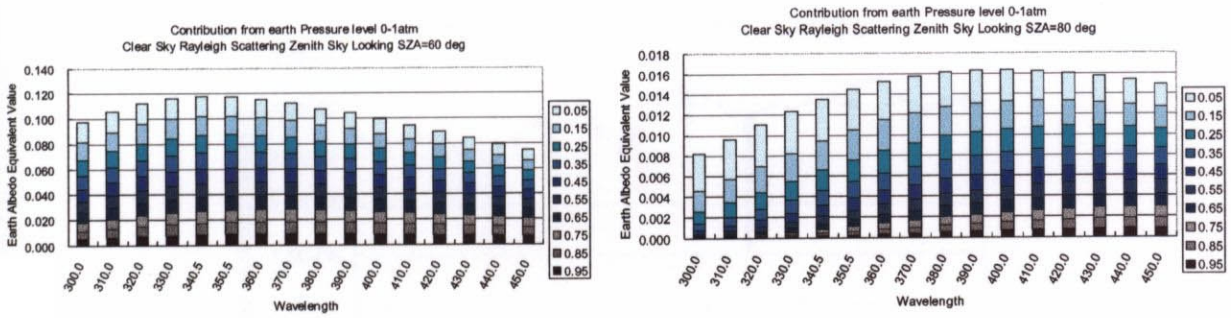

Figure 5-27. The spectral characteristics models of each layer contribution for the solar zenith angles of 60 deg (left) and 80 deg (right).

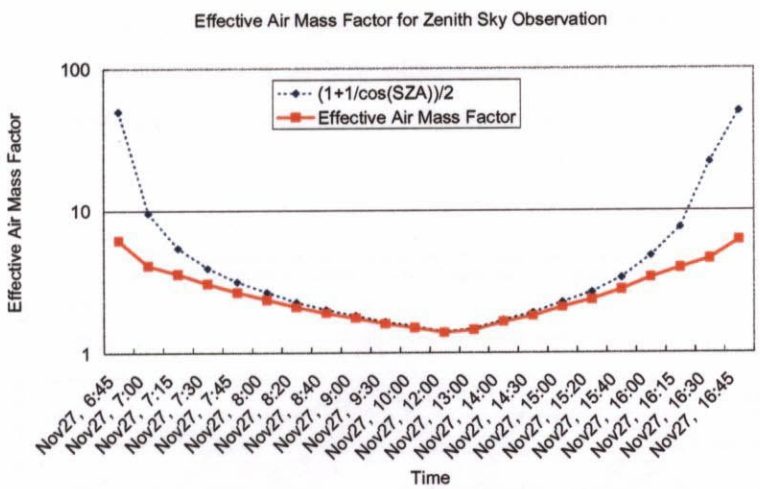

Figure 5-28. Effective air-mass factor at 420 nm of November 27, 2002 observation.

(4) Pair method

The vertical column density of NO_2 can be retrieved by using the sensitive and insensitive spectral bands. Figure 5-29 depicts the convoluted spectra with solar Fraunhofer lines and the instrument function and the center wavelength positions of each pixel. The figure indicates that the Fraunhofer spectra themselves have structure and that the observed spectra must be carefully corrected. Figure 5-30 presents the diurnal variation. The retrieved value is corrected using the effective air-mass factor described in Figure 5-28.

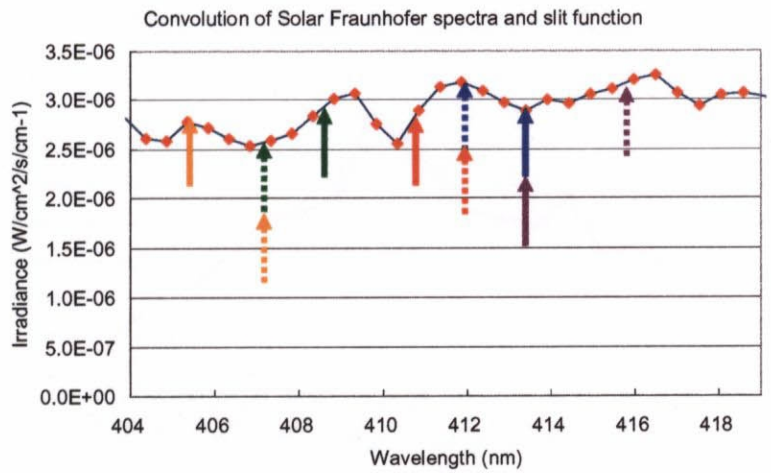

Figure 5-29. Fraunhofer spectra between 404-419 nm where NO_2 is retrieved and the wavelength position of the pairs of NO_2 differential absorption retrieval. The arrows indicate the sensitive and insensitive pairs of NO_2 absorption.

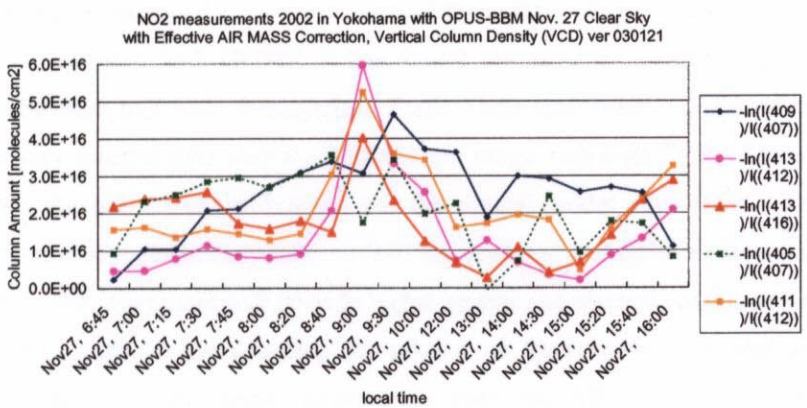

Figure 5-30. Diurnal variation of retrieved vertical column density of NO_2 from pairs method (differential absorption method) in Yokohama on November 27, 2002.

(5) Spectral fitting and retrieved results

Spectral fitting is necessary to improve the retrieval accuracy since both the column amount of NO_2 and the difference of the NO_2 absorption cross section are small. Figure 5-31 illustrates the retrieved diurnal variation measured at a plant near a road with heavy traffic. The increase of the NO_2 amount around 9:00 AM is due to local air pollution caused by emission from the heavy traffic. The attenuation in the afternoon is due to dilution caused by wind from the sea, which is about 10 km away from the measurement location.

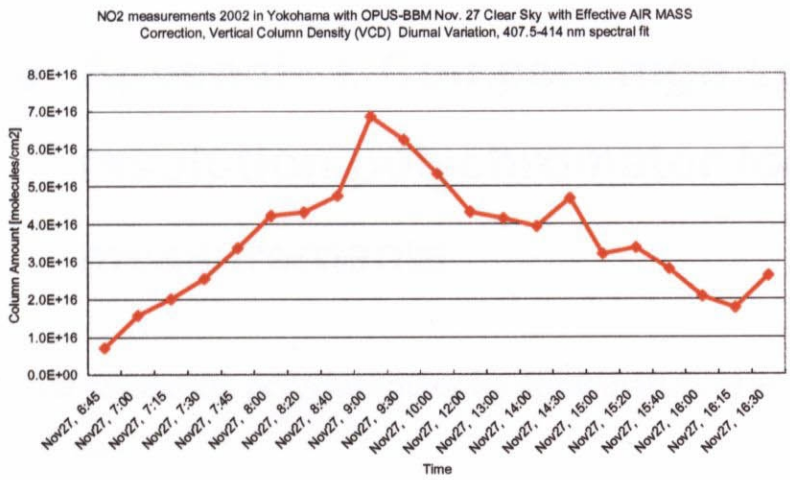

Figure 5-31. Diurnal variation of the retrieved vertical column density of NO_2 using spectral fitting method in Yokohama on November 27, 2002.

5.8. Conclusion of this Chapter

The UV spectrometer discussed here has the optical throughput of $1e^{-8}$ m^2str, which about 4 times larger than that of TOMS. Compared with GOME, it has almost the same throughput and much higher spatial resolution. The combination of a well-characterized Fastie-Ebert spectrometer and a custom CMOS detector will provide high fidelity spectral data over the 300-452 nm range with high SNR. The slit function will be characterized by both the pre-launch calibration and the optical model simulation. The wavelength and response will be calibrated using a Hg lamp with +/- 0.01 nm accuracy and diffuser plates onboard, respectively for the entire mission. The instrument will provide higher spatial and spectral resolution data than the existing instruments, and so will improve the accuracy of retrieval of the total O_3. In addition, cloud detection radiometers will provide the cloud height information from the effective path length. Therefore, the tropospheric NO_2, SO_2, O_3, and minor constituents will be extracted. The ground-based observation proved the performance of high SNR, high spectral resolution, and uniform slit function of both UV polychromator and O_2 *A* band filter radiometer.